Journal of
Manufacturing and Materials Processing

MDPI

Article

Stiffness Enhancement by Means of Situational Coupling of Two Collaborative Robots

Eckart Uhlmann [1,2], Marie-Noëlle Fielers [1,*], Thomas Pache [1] and Onur Senyüz [1]

[1] Institute for Machine Tools and Factory Management IWF, Technische Universität Berlin, Pascalstraße 8-9, 10587 Berlin, Germany
[2] Fraunhofer Institute for Production Systems and Design Technology IPK, Pascalstraße 8-9, 10587 Berlin, Germany
* Correspondence: marie.fielers@iwf.tu-berlin.de

Abstract

While collaborative robots are designed to enable flexible and safe human–robot interactions, their comparatively low structural stiffness poses a challenge for high-precision machining and heavy-assembly tasks. Addressing this limitation is essential for enhancing their performance and improving their overall efficiency in manufacturing processes. This paper proposes an approach for enhancing the stiffness by means of situational coupling of two collaborative robots. Therefore, an analysis is conducted to determine the kinematic limitations of coupled collaborative robots. The stiffness of coupled collaborative robots is then modeled using the finite element method. Furthermore, experimental stiffness measurements of a single collaborative robot are conducted to establish a quantitative reference, which is both to validate the model and to quantify the stiffness enhancement achieved through coupling. On the basis of the combined experimental and numerical results, it is demonstrated that the approach of coupling has the potential to enhance stiffness by up to 37.19 times in comparison with a solitary collaborative robot.

Keywords: collaborative robots; stiffness; robot cooperation

Academic Editor: Edouard Rivière-Lorphèvre

Received: 1 December 2025
Revised: 30 January 2026
Accepted: 2 February 2026
Published: 4 February 2026

Correction Statement: This article has been republished with a minor change. The change does not affect the scientific content of the article and further details are available within the backmatter of the website version of this article.

1. Introduction

Flexible process automation is playing an increasingly decisive role in the economic competitiveness and sustainability of modern production systems [1]. Due to global market volatility, rising production costs and demographic changes, the use of robots is becoming progressively more important to ensure efficiency gains and production reliability. This is reflected in the continuously rising annual installation rate of robots. This amounted to over 500,000 units each year from 2021 to 2023, and further acceleration of this growth is forecast for the coming years [2]. Collaborative robots (cobots), in particular, are gaining importance due to their unique advantages, the most significant of which is their capability for direct and safe human–robot interaction—a key distinction from industrial robots [3]. This is also reflected in their steadily increasing market share, which reached almost 10% of total robot sales in 2023 [2].

Despite these advantages, the comparably low structural stiffness k of cobots remains one of the major challenges for their application in high-precision machining processes and assembly work with high process forces F_P. Low structural stiffness k can lead to deformations that negatively impact machining speed, process stability and energy efficiency. The open kinematic chain of a serial six-axis cobot causes the structure to bend,

similar to a machine tool frame in C-design, which leads to a deterioration in the pose accuracy T at the tool center point (TCP) and, thus, to errors in the execution of the cobot's task, see Figure 1a.

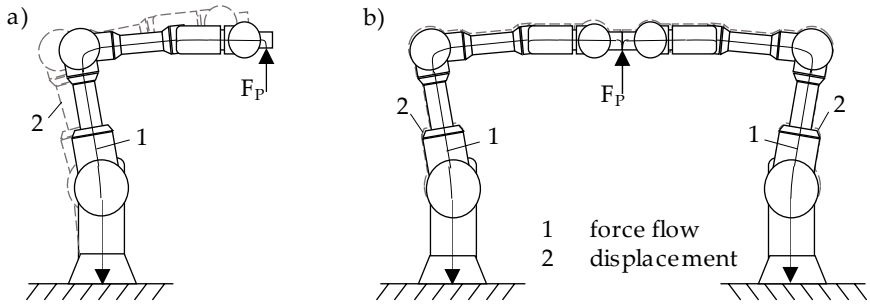

Figure 1. Force flow and displacement: (**a**) Open kinematic chain of a 6-axis cobot; (**b**) closed kinematic chain of coupled cobots.

Higher structural stiffness k not only improves the pose accuracy T, payload capacity and process stability but also extends the range of industrial tasks that cobots can reliably perform, and thus, facilitates a more flexible and safe production. Numerous research projects, therefore, focus on increasing structural stiffness k, where a distinction can be made between design and compensatory measures. Design measures focus on increasing structural stiffness k by modifying the robot structure. Implementation of these measures is generally only possible retrospectively or iteratively, if at all, by means of extensive conversion work. According to Brecher et al. [4], the differentiation of robots in terms of their kinematics can be categorized into three distinct classifications: open, closed and partially closed chains. The serial arrangement of arm members and the resulting long, cantilevered arm structure result in open kinematic chains that exhibit low structural stiffness k. Integration of a parallelogram mechanism between axes two and three alleviates the load on the drive of axis two, thereby enhancing the structural stiffness k and positional accuracy T of the robot [5]. However, the closed kinematic sub-chain imposes constraints on flexibility and working space. Completely closed kinematic chains are also characterized by high structural stiffness k with lower flexibility and mobility. In this context, Tanev, Yeshmukhametov et al., and Fang et al. investigated hybrid serial–parallel kinematic chains [6–8]. Wang et al. [9] present an elastostatic-stiffness modeling approach for hybrid robotic structures, in which the parallel and serial modules can be analyzed separately. In contrast, numerous robot manufacturers prioritize increasing the robot arm's cross-section to enhance its structural stiffness, as evidenced by the findings of Wu et al. [10]. However, an increase in the arm's cross-section results in an elevated dead weight, concurrently compromising the robot's dynamic performance. Chen et al. [11] present a modeling approach that simulates robot stiffness considering joint flexibility through a rigid–flexible coupling. Time-varying stiffness models are developed and applied for trajectory planning. An alternative approach was presented by Lai et al. [12], where two serial 3-axis industrial robots were permanently connected. The main structure is equipped with a spindle at the end effector. The support structure is attached to the end effector of the main structure. During the machining process, the support structure is anchored to a fixed point within in the working space. In this configuration, the system employs parallel kinematics with serial arms. In this coupled operating state, a parallel connection of the two Cartesian stiffnesses k_{kart} of the serial arms has been postulated in regard to the structural stiffness k. Conversely, compensatory measures are intended to enhance positional accuracy T without the need for structural modifications. The prevailing focus of research in this field is the development of globally applicable compensation measures. These measures are

based on models that describe the causes of error in the robot's kinematic model [13–15]. Depending on the complexity of the models under consideration, Roth et al. [16] introduced a distinction between three calibration categories:

- Level-1 calibration:
  → Compensation for joint axis angle errors,
- Level-2 calibration:
  → Compensation for geometric errors (regarding angle errors and arm lengths),
- Level-3 calibration:
  → Compensation for non-geometric errors (e.g., elastic and thermal deformations, friction, gear backlash, gear ratio errors).

As demonstrated in numerous studies, the implementation of a level-2 calibration results in a 90% enhancement in positional accuracy T [17]. However, it proves inadequate for processes characterized by high process forces F_P and accuracy requirements due to the low structural stiffness k. While the gradual increase in model complexity enhances model quality, it concurrently complicates parameter identification. Furthermore, the complexity of the model is constrained by the necessity of a sufficiently brief calculation time.

In light of the aforementioned context, this paper proposes an innovative approach to improving the stiffness k by means of situational coupling of two six-axis cobots. Due to the optimized force flow in the coupled operating state, a significant increase in stiffness k is expected, similar to a machine tool in O-design, seen in Figure 1b. Coupling of industrial robots is proposed by Goebels et al. [18], Neusser et al. [19], Mühlbeier et al. [20] and Ye et al. [21]. Notably, Ye et al. [21] demonstrated experimentally that stiffness-oriented cooperative placement and motion planning for physically coupled industrial robots is feasible and beneficial in manufacturing contexts. However, these studies are limited to conventional industrial robots. The systematic coupling of cobots has not yet been explored, and the characteristic features of cobots fundamentally impose different requirements for achieving safe and fully synchronized cobot coupling [22]. Most importantly, the lightweight and compliant design, driven by safety requirements, is a key characteristic of cobots and should be preserved. Therefore, it is essential to specifically enhance the structural stiffness k through the coupling of two cobots in order to ensure precise and stable collaboration without compromising their fundamental safety advantages.

2. Concept for the Situational Coupling

From the results of the aforementioned studies concerning the coupling of conventional industrial robots, it is assumed that situational coupling in the overlapping workspace of two cobots offers the opportunity of direct integration of tasks with high process force F_P and accuracy requirements. Therefore, it is hypothesized that such a configuration will enhance flexibility in cobot-based process chains, thereby facilitating automation and increasing productivity, even with small batch sizes. The concept investigated in this paper is based on two cobots working independently in a decoupled mode while remaining within mutual reach. Since such configurations are already present in many industrial cobot-based process chains, the proposed approach can be readily integrated into existing industrial environments. When a process task requires a stiffness exceeding the achievable stiffness of a single cobot, mechanical coupling is activated to form a serial–parallel system. The switching criterion is defined by a task-dependent stiffness requirement k_{req}, which is compared to the estimated single-cobot stiffness k_{single} in the current configuration. Coupling is initiated when $k_{req} > k_{single}$ and released once $k_{req} \leq k_{single}$. This strategy ensures that mechanical coupling is applied only when necessary, providing high stiffness k during force-critical phases, while maintaining the advantages of collaborative operation

during all other phases. The stiffness requirement k_{req} is derived from the task description and online process monitoring. When the condition $k_{req} > k_{single}$ is detected, the system automatically triggers the coupling mechanism. After completing its current task, the secondary cobot moves into position and establishes the mechanical connection, forming a coupled system. Once the force-critical phase is completed and the stiffness required k_{req} falls below the single cobot stiffness k_{single}, the system autonomously decouples and returns to compliant single-cobot operation. This way, the approach ensures that both cobots maintain their inherent high degree of flexibility and dynamics in the decoupled operating state, see Figure 2.

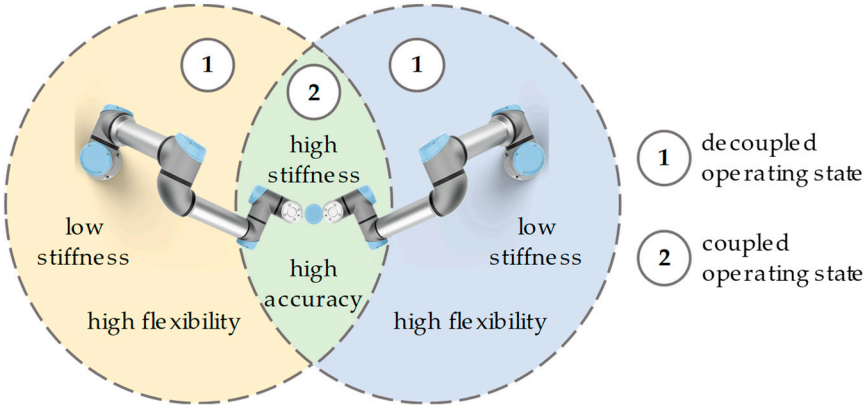

Figure 2. Organizing the working space of cooperating cobots according to the requirements.

This requires the use of a flexible coupling interface, which enables a fully automated coupling and decoupling process of both cobots and fulfills the conflicting requirements of lightweight construction, high stiffness, high precision and low costs. Furthermore, the native control system of both cobots has to be adapted. It is essential to ensure that both cobots follow a synchronized trajectory.

The proposed situational coupling strategy is particularly well-suited for robotic tasks that are characterized by alternating phases of high compliance and high stiffness demand. Typical examples include contact-rich operations such as surface finishing, grinding, or precision assembly. In these tasks, high stiffness k is required only during specific process phases, while flexible behavior remains advantageous, e.g., during approach and positioning. However, tasks that demand high positioning accuracy at high dynamic speeds may be limited by the dynamic coupling effects introduced by the second robot and the coupling interface.

3. Kinematic Model for the Coupled Operating State

In order to both coordinate the cobots in the coupled operating state and to generate possible joint angle configurations for the stiffness model, a mathematical representation of the coupled kinematics is required. The cooperative cobot system is considered a combination of two serial cobots, I, $I \in \{A \mid B\}$. In addition to the two Cartesian base coordinate systems K_I, $I \in \{A \mid B\}$, a working coordinate system K_x is introduced. The constant homogeneous transformation matrix ${}^{X}_{I}\mathbf{T}$ represents the rotation and displacement of K_x relative to K_I. The homogeneous transformation matrix between the base coordinate system and the end effector flange ${}^{EE\_I}_{I}\mathbf{T}$ can be determined according to Formula (1).

$$ {}^{EE\_I}_{I}\mathbf{T} = {}^{X}_{I}\mathbf{T} \cdot {}^{AP}_{X}\mathbf{T} \cdot {}^{EE\_I}_{AP}\mathbf{T} = \begin{pmatrix} {}^{I}\mathbf{R}_{K_I \to EE\_I} & {}^{I}\mathbf{x}_{K_I \to EE\_I} \\ 0 & 1 \end{pmatrix}, \quad (1) $$

In Formula (1), ${}^{AP}_{X}\mathbf{T}$ represents the homogeneous transformation matrix between the working coordinate system and the working point, while ${}^{EE\_I}_{AP}\mathbf{T}$ represents the homogeneous transformation matrix between the working point and the end effector flange of the cobot. Figure 3 illustrates the definitions of the homogeneous transformation matrices.

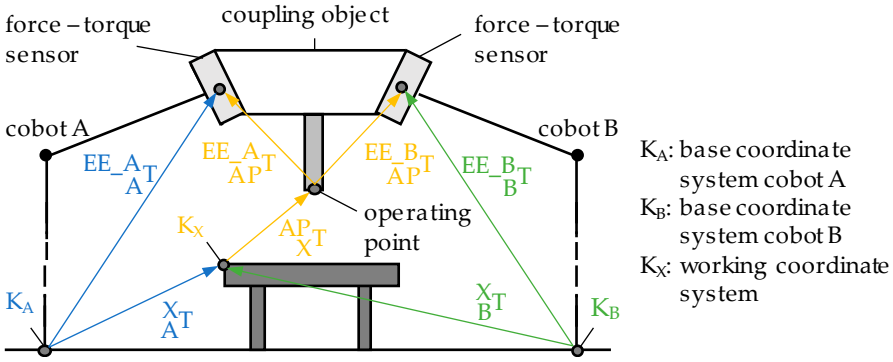

Figure 3. Kinematics of two cobots in coupled operating state.

The so-defined coupled kinematics was implemented in the software MATLAB R2023b of the company The Mathworks Inc., Natick, MA, USA. Figure 4 exemplifies the resulting coupled working space given a base distance d_h = 1500 mm.

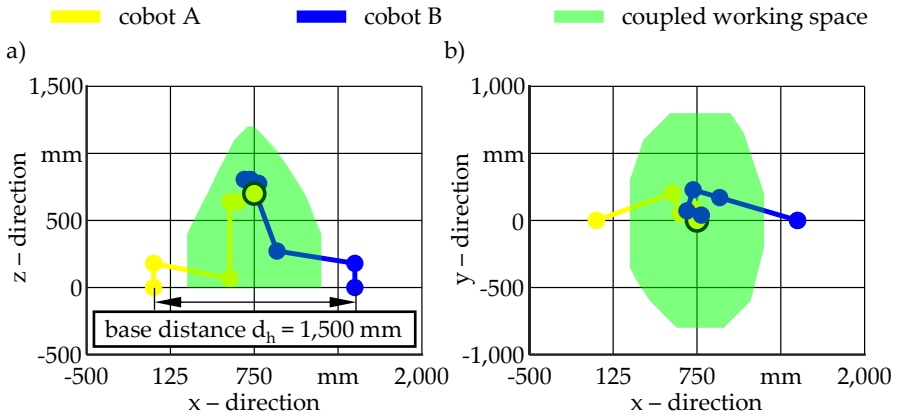

Figure 4. Simulated working space of two coupled cobots: (**a**) X–Z view; (**b**) X–Y view.

For modeling purposes, the forward and backward kinematics of the cobot of type UR10e from the company Universal Robots A/S, Odense, Denmark, were implemented. For the sake of simplicity, it will be referred to as UR10e from here on out. Since the end effectors of the cobots should be connected to each other, preventing any relative motion, a point constraint was defined accordingly. The distance between the base coordinate systems of the cobots was set to d_h = 1500 mm, as this provides the optimal ratio of workspace to installation area. The maximum working space between the cobots corresponds to the maximum reach of the cobots, which is l_{UR10e} = 1300 mm. Evidently, due to inherent structural limitations, including the diameter of the cobot's base d_b = 190 mm, a base distance d_h = 1300 mm is infeasible. To ensure sufficient space, this results in a base distance of d_h = 1500 mm. Consequently, the resulting working space volume is determined to be $V_{A,coup}$ = 1.06 m^3. Comparing the usable working space volume of a single UR10e, $V_{A,UR10e} \approx 3.50$ m^3, with that of the coupled cobots reveals that the latter is only about 30.23%. In order to avoid noticeable loss of flexibility through permanent coupling, the implementation of fully automated coupling mechanisms is of crucial importance. This enables either a high degree of flexibility or high stiffness k to be achieved, depending on the requirements of the application.

4. Stiffness Tests of the Cobot

In order to enable an increase in system stiffness k throughout the coupling of cobots, it is essential to investigate the stiffness k of a single UR10e. Therefore, stiffness tests were carried out. According to the manufacturer's datasheet, the UR10e's maximum payload capacity is $m_{P,UR10e}$ = 12.50 kg. Its reach measures to $l_{R,UR10e}$ = 1300 mm and its net weight to $m_{E,UR10e}$ = 33.50 kg [23].

4.1. Experimental Procedure

To determine the stiffness k of the UR10e, a radial force F_{rad} is applied to its end effector, and the corresponding displacement u of the end effector is measured. To carry out the tests, the end effector of the UR10e is moved to a specific position. This position along the base coordinate system's x-axis corresponds both to the UR10e's nominal operational configuration and to the midpoint of the simulated working space. The positions in the y- and z-directions remained invariant, due to the given environmental conditions. The stiffness measurement was performed in this deliberately selected reference configuration, which is kinematically extended and located in a mid-workspace region known to be among the most compliant and critical for serial manipulators. Since the objective of this work is to demonstrate the achievable stiffness gain through coupling, this pose represents a conservative and representative test case. While the absolute stiffness k of a single robot varies over the workspace, the relative stiffness gain introduced by mechanical coupling is primarily determined by the serial–parallel topology and is, therefore, largely independent of the specific robot pose. Consequently, the measured stiffness increase can be interpreted as a representative indicator of the coupling effect. During the application of the radial force F_{rad} at the designated operating point, the UR10e is in switched-on mode without performing any movement, so that the experiments could be conducted under quasistatic conditions. The radial force F_{rad} is applied to the UR10e's end effector in the respective opposite direction from which it has been moved to its target position. A type 9257B multi-component dynamometer from the company Kistler Group, Winterthur, Switzerland, is used to measure the radial force F_{rad}. The radial force F_{rad} is calculated using the LabVIEW interface from the company National Instruments, Austin, TX, USA, and is applied by a fine-thread screwing device, which is connected to the multi-component dynamometer by a screw connection. The displacement u of the end effector is measured using a laser triangulator of the type ILD2200-10 from the company MICRO-EPSILON Optronic GmbH, Dresden, Germany. Both radial force F_{rad} and displacement u are recorded at a sampling rate of f_s = 1 Hz. The stiffness k was identified under quasistatic loading conditions, where the robot was allowed to settle after each force increment. Therefore, a sampling rate of f_s = 1 Hz is sufficient, as no dynamic effects were evaluated and all measurements correspond to static equilibrium points. The entire measurement procedure was repeated three times. Figure 5 illustrates the experimental setup.

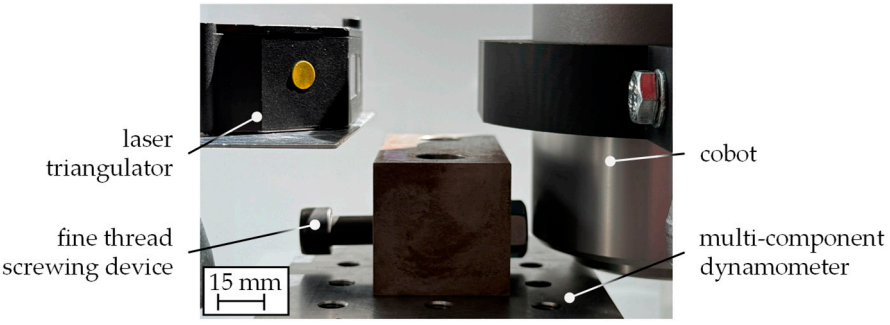

Figure 5. Experimental setup for stiffness tests with a UR10e.

4.2. Results and Evaluation

Figure 6 shows the mean values of the measured displacement u in the x- and y-directions, subject to radial force F_{rad} imposed on the end effector, along with the respective standard deviation. In order to determine the in-plane and out-of-plane stiffness k of the UR10e, radial forces F_{rad} were applied in both the x- and y-directions, the amplitude of which ranged up to two orders of magnitude. Utilizing a weighted least square algorithm, the average stiffness of k_x = 95.94 N/mm in the x-direction and k_y = 57.42 N/mm in the y-direction was obtained on the basis of the three repetitions. Thus, the UR10e exhibits a structural stiffness k that is about 67% higher in the x-direction than in the y-direction.

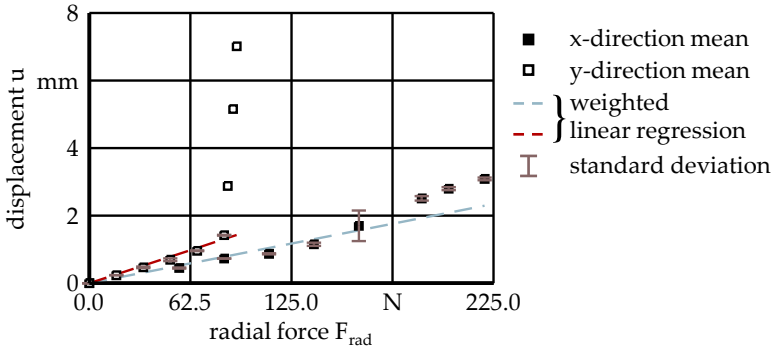

Figure 6. Displacement–force diagram for measurements conducted with the UR10e.

The maximum displacement in the x-direction, $u_{x,max} \approx 3.09$ mm, occurred at the corresponding maximum radial force of $F_{rad,x,max} \approx 220$ N. In accordance with a priori expectations, the UR10e demonstrated a capacity of a maximum radial force of only $F_{rad,y,max} \approx 82$ N in the y-direction, resulting in a displacement of $u_{y,max} \approx 7.01$ mm. This is consistent with the observations made during the experiments, where at a threshold of radial force $F_{rad,y} \approx 75$ N and displacement $u_y \approx 1.42$ mm, any additional rotation of the fine-thread screwing device would result in only a slight increase in the measured radial force $F_{rad,y}$, while a substantial increase in the corresponding displacement u_y occurred. In the x-direction, the same amplitude of radial force F_{rad} resulted in a displacement of merely u_x = 0.73 mm. To characterize these spatial differences in the UR10e's behavior, the pointwise stiffness k_{pw}, as defined in Formula (2), was determined.

$$k_{pw,i} := \frac{\Delta F_{rad}}{\Delta u} = \frac{F_{rad,i+1} - F_{rad,i}}{u_{i+1} - u_i} \quad (2)$$

Figure 7, accordingly, illustrates the mean values of pointwise stiffness k_{pw} in the x- and y-directions, subject to radial force F_{rad} imposed on the end effector, along with the respective standard deviation.

The observed anisotropy in the stiffness k may be attributed to the UR10e's kinematic structure, in particular the general arrangement and alignment of its joints and the resulting transmission of force and momentum, as well as the pose under consideration within the conducted tests.

4.3. Stiffness Evaluation of Cobots in Coupled Operating State

To investigate the effect of coupling two cobots on compound stiffness k_C, a simulation-based analysis was conducted. For this purpose, a multibody simulation model was implemented in the finite element software Ansys 2025 R2 provided by the company Ansys Inc., Canonsburg, PA, USA. In order to obtain general insights into the overall effect, certain assumptions have been made, e.g., the simplification to a quasistatic problem due to slow force application, negligible influence of material properties as all arms are assumed to be

stiff and discrete localization of all compound compliances s_C in the six or twelve cobot joints, respectively [24]. The joints were configured as purely rotational, with one degree of freedom each, and independent torsional stiffnesses $c_{T,i}$. These torsional stiffnesses $c_{T,i}$ were utilized as parameters for phenomenologically adjusting the behavior of a single cobot. Therefore, experimental data presented in Section 4.2 have been reproduced by numerically varying each joint's torsional stiffness c_T. In the coupled operating state, the coupling object between the two cobots was modeled as stiff, preventing any relative motion between the end effectors and reflecting a typical state of pre-tension in these components, seen in Figure 3. Boundary conditions at the bases were set according to the fixed clamping of both cobots to the ground. The model has been implemented such that the second cobot is mirrored to the first one with respect to the y'z-plane, resulting in a relative angle of $\alpha = 107°$, seen in Figure 8.

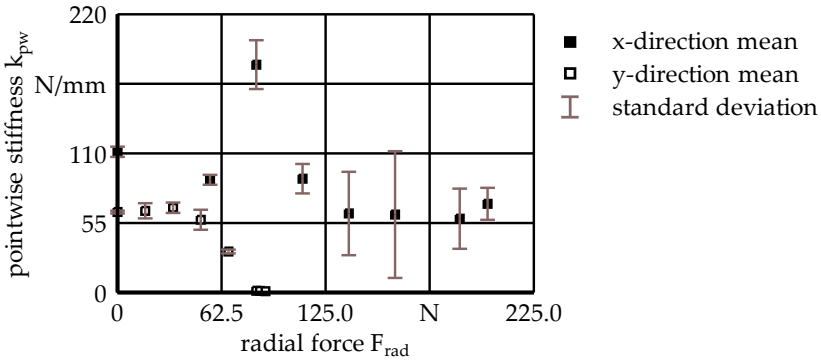

Figure 7. Pointwise stiffness k_{pw} of the UR10e at the different levels of radial force F_{rad} under consideration.

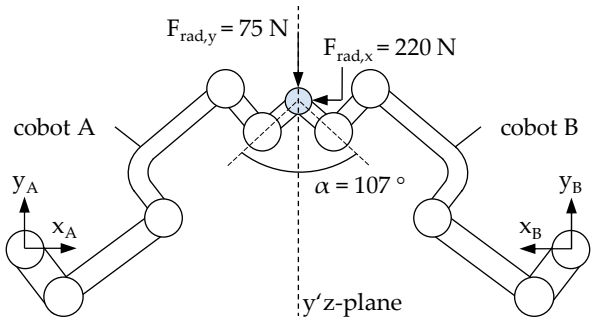

$F_{rad,y}$: radial force in y-direction $F_{rad,x}$: radial force in x-direction

Figure 8. Schematic of the finite element model in single and coupled operating state.

Loading was configured according to single-cobot experiments as stated in Section 4.2 and was applied to the common node of the end effectors. The simulation could prove the exemplary expediency of the concept; as in the coupled operating state, increased compound stiffnesses of $k_{C,x} \approx 212$ N/mm and $k_{C,y} \approx 2.95$ kN/mm were observed. An additional simulation, besides the stiff-beam model, was conducted, in which the coupling object shown in Figure 3 is modeled as a compliant beam. Figure 9 illustrates the differences in compound stiffness k_{cx} and k_{cy} between the compliant beam, the stiff beam, and the experimental measurements. The actual coupling mechanism has not yet been developed, but it is expected to exhibit an effective stiffness that lies between the two considered extremes, namely, compliant and stiff simulated behavior, due to mechanical preloading and the constrained and interlocked kinematic structure. It should be noted that an additional side effect of the angled arrangement is that both cobots compensate for the

more compliant spatial direction of the other. This results in an overall stiffer structure, as the results illustrate.

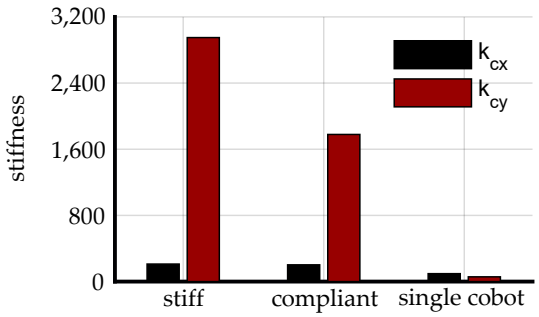

Figure 9. Stiffness comparison between the stiff-beam model, the compliant-beam model and the experimental results of the single cobot.

5. Conclusions

In this paper, the concept of situational coupling of two cobots was presented. For this purpose, the resulting working space of the coupled cobots was determined by a kinematic model. Furthermore, pose-related stiffness in the planar main-axis system of a single cobot of type UR10e was investigated experimentally. Therefore, radial forces $F_{rad,i}$ in the x- and y-directions were applied to the UR10e's end effectors, and the resulting displacement u_i was measured. The results of the analysis yield a stiffness ratio of $\eta = k_x/k_y \approx 1.67$ with respect to the UR10e's base coordinate system.

Next, a multibody simulation model of the UR10e was implemented and parameterized digitally, utilizing experimentally obtained measurement data. The adapted parameter values then were used to numerically investigate the coupling of two UR10e. The compound stiffnesses $k_{C,i}$ exhibited an enhancement in comparison to the single operating state, with an increase of approximately 200% in the x-direction and approximately 5940% in the y-direction. In light of these findings, an angular arrangement of the two cobots was found to be advantageous in terms of compensating for the respective more compliant direction of movement. These findings substantiate the conceptual viability of situationally coupled cobots and indicate the necessity for further research to investigate the scope of applications in which the structural advantages of collaborative industrial robots can be leveraged. Future research, therefore, may aim to extend this investigation throughout the entire working space, incorporating stiffness characteristics of the cobots' arm segments. Furthermore, the determination of an optimal angle α in the coupled operating state with regard to compound stiffness k_C and optimal pre-tension of the end effectors represent potential subjects for further investigation.

Author Contributions: Conceptualization, M.-N.F. and O.S.; methodology, writing—original draft preparation, formal analysis, visualization, M.-N.F.; software, validation, data curation, M.-N.F. and T.P.; writing—review, E.U.; supervision, project administration, funding acquisition, E.U. All authors have read and agreed to the published version of the manuscript.

Funding: This research was funded by the German Federal Ministry for Economic Affairs and Energy and the project organizer VDI/VDE Innovation + Technik GmbH, grant number 16TNW0008E. We acknowledge support by the Open Access Publication Fund of TU Berlin.

Data Availability Statement: The raw data supporting the conclusions of this article will be made available by the authors on request.

Conflicts of Interest: The authors declare no conflicts of interest.

References

1. International Federation of Robotics (IFR). *World Robotics Report*; International Federation of Robotics: Frankfurt, Germany, 2023.
2. Müller, D.C. *World Robotics Industrial Robots 2024*; VDMA Services GmbH: Frankfurt, Germany, 2024. Available online: https://ifr.org/img/worldrobotics/Executive_Summary_WR_2024_Industrial_Robots.pdf (accessed on 28 March 2025).
3. Patil, S.; Vasu, V.; Srinadh, K.V.S. *Advances and Perspectives in Collaborative Robotics: A Review of Key Technologies and Emerging Trends*; Discover Mechanical Engineering: Warangal, India, 2023.
4. Brecher, C.; Dannenmann, E.; Dorn, L.; Pritschow, G.; Siegert, K.; Spur, G.; Grote, K.-H. (Eds.) *Dubbel*, 22. Aufl. s.l.; Springer: Berlin/Heidelberg, Germany, 2007.
5. Reinkober, S. Fräsbearbeitung von Nickelbasislegierungen Mit Industrierobotern. Ph.D. Thesis, Fraunhofer-Institut für Produktionsanlagen und Konstruktionstechnik, Berlin, Germany, 2017.
6. Tanev, T.K. Kinematics of a hybrid (parallel–serial) robot manipulator. *Mech. Mach. Theory* **2000**, *35*, 1183–1196. [CrossRef]
7. Yeshmukhametov, A.; Kalimoldayev, M.; Mamyrbayev, O.; Amirgaliev, Y. Design and kinematics of serial/parallel hybrid robots. In Proceedings of the 2017 3rd International Conference on Control, Automation and Robotics, Nagoya, Japan, 24–26 April 2017; pp. 162–165.
8. Fang, L.; Liang, F.; Sun, L. Comparative Study of Stiffness Modeling Methods for A Novel Industrial Robotic Arm with Hybrid Open- and Closed-Loop Kinematic Chains. In Proceedings of the 2018 IEEE International Conference on Mechatronics and Automation (ICMA), Changchun, China, 5–8 August 2018; pp. 1765–1770.
9. Wang, B.; Li, P.; Yang, C.; Hu, X.; Zhao, Y. Robotica: Decoupled elastostatic stiffness modeling of hybrid robots. *Robotica* **2024**, *42*, 2309–2327. [CrossRef]
10. Wu, K.; Li, J.; Zhao, H.; Zhong, Y. Review of Industrial Robot Stiffness Identification and Modelling. *Appl. Sci.* **2022**, *12*, 8719. [CrossRef]
11. Chen, J.; Liu, Z.; Chen, C.; Qi, B.; Xu, J.; Tao, L.; Yan, Q. Robot stiffness modeling based on the rigid flexible coupling simulation and its application to trajectory planning. *Precis. Eng.* **2025**, *92*, 77–89.
12. Lai, C.Y.; Villacis Chavez, D.E.; Ding, S. Transformable parallel-serial manipulator for robotic machining. *Int. J. Adv. Manuf. Technol.* **2018**, *97*, 2987–2996. [CrossRef]
13. Weigold, M. Kompensation der Werkzeugabdrängung bei der Spanenden Bearbeitung Mit Industrierobotern. Ph.D. Thesis, Technische Universität Darmstadt, Darmstadt, Germany, 2008.
14. Klimchik, A. Enhanced Stiffness Modeling of Serial and Parallel Manipulators for Robotic-Based Processing of High Performance Materials. Ph.D. Thesis, Ecole Centrale de Nantes, Nantes, France, 2012.
15. Peng, J.; Ding, Y.; Zhang, G.; Ding, H. An enhanced kinematic model for calibration of robotic machining systems with parallelogram mechanisms. *Robot. Comput.-Integr. Manuf.* **2019**, *59*, 92–103. [CrossRef]
16. Roth, Z.; Mooring, B.; Ravani, B. An overview of robot calibration. *IEEE J. Robot. Autom.* **1987**, *3*, 377–385. [CrossRef]
17. Renders, J.-M.; Rossignol, E.; Becquet, M.; Hanus, R. Kinematic calibration and geometrical parameter identification for robots. *IEEE Trans. Robot. Autom.* **1991**, *7*, 721–732. [CrossRef]
18. Goebels, M.; Baumgärtner, J.; Fuchs, T.; Mühlbeier, E.; Puchta, A.; Fleischer, J. Milling using two mechatronically coupled robots. In Proceedings of the 57th CIRP Conference on Manufacturing Systems CMS 2024, Karlsruhe, Germany, 29–31 May 2024.
19. Neusser, Z.; Valasek, M.; Necas, M. Stiffness Increase and Homogenization by Coupled Robots. *Mech. Based Des. Struct. Mach.* **2025**, *53*, 3572–3589.
20. Mühlbeier, E.; Bauer, V.; Schade, F.; Gönnheimer, P.; Becker, J.; Fleischer, J. Mechatronic Coupling System for Cooperative Manufacturing with Industrial Robots. In Proceedings of the 56th CIRP Conference on Manufacturing Systems, Capetown, South Africa, 24–26 October 2023.
21. Ye, X.; Schwartz, M.; Hohmann, S. Stiffness Optimized Multi-Robot Behavior Planning Using Reduced Hessian Method. *IFAC-Pap. OnLine* **2022**, *55*, 55–60.
22. Kulkarni, A.; Raut, R.; Dhatrak, P. A comprehensive review on configuration, design and programming of robotic systems used in various applications. *Int. J. Intell. Robot. Appl.* **2025**, *9*, 1187–1213. [CrossRef]
23. Universal Robots Homepage: UR10e Technische Daten. Available online: https://www.universal-robots.com/media/1811481/ur10e-product-factsheet-de-web.pdf (accessed on 17 April 2025).
24. Spong, M.W.; Hutchinson, S.; Vidyasagar, M. *Robot Modeling and Control*, 2nd ed.; John Wiley & Sons: Hoboken, NJ, USA, 2020.